

Article

Characteristics of Flame Stability and Gaseous Emission of Bio-Crude Oil from Coffee Ground in a Pilot-Scale Spray Burner

Sang Kyu Choi ^{1,2,*}, Yeon Seok Choi ^{1,2}, Yeon Woo Jeong ¹, So Young Han ¹  and Quynh Van Nguyen ²

¹ Department of Clean Fuel & Power Generation, Korea Institute of Machinery and Materials, 156 Gajeongbuk-ro, Yuseong-gu, Daejeon 34103, Korea; yschoi@kimm.re.kr (Y.S.C.); ywjeong@kimm.re.kr (Y.W.J.); syhan@kimm.re.kr (S.Y.H.)

² Environment & Energy Mechanical Engineering, University of Science and Technology, 217 Gajeong-ro, Yuseong-gu, Daejeon 34113, Korea; josquynhvn@kimm.re.kr

* Correspondence: skchoi4091@kimm.re.kr; Tel.: +82-42-868-7398

Received: 4 May 2020; Accepted: 31 May 2020; Published: 4 June 2020



Abstract: Coffee ground has been recently considered as a new biomass resource in relation to the increasing coffee consumption worldwide. The bio-crude oil can be produced by fast pyrolysis of coffee ground, and it has advantages of larger heating values in comparison with those from other biomass. But the bio-crude oil from coffee ground has a significantly high viscosity which can hinder the application to conventional burners. In this study, a pilot-scale burner system with a 35 kW capacity with an air-blast atomizing nozzle was developed for the combustion of bio-crude oil from coffee ground with a high viscosity. A downward fuel injection system was adopted to enhance the ignition of fuel spray and the flame stabilization, and a movable block swirl generator was installed for the combustion air. The bio-crude oil was blended with ethanol at the volumetric ratio of 9:1 to enhance the combustion characteristics. The effect of various atomizing air pressures, swirl intensities, and overall equivalence ratios on the flame stability and gaseous emission were investigated to find out the optimum operating conditions for a bio-crude oil burner.

Keywords: coffee ground; bio-crude oil; burner; flame stability; gas emission

1. Introduction

The utilization of renewable energy has been recently studied with much attention to resolve the global environmental problems including fossil fuels and global warming. Biomass can be one of the promising renewable energy sources because of its carbon neutrality in the combustion process. The utilization of biomass by direct combustion could be hardly adopted in the aspects of fine dust emissions, which can be reduced by using liquid fuel. Furthermore, the energy density is increased by converting biomass into liquid fuel which facilitates efficient storage and transportation. Bio-crude oil can be produced by the fast pyrolysis of various kinds of biomass. At a temperature around 500 °C and in an oxygen-free environment, biomass particles are decomposed into gas phase and retained solid phase with a short residence time of less than 2 s. The volatile in the gas phase are condensed into the bio-crude oil [1–4].

Woody biomass and herbaceous plants have been generally studied as feedstocks for fast pyrolysis, and the produced bio-crude oil has a complex composition depending on the biomass feedstock. It is known that the water content of bio-crude oil ranges from 15% to 30% by weight, and the calorific value is typically 14–18 MJ/kg which corresponds to 50%–60% of energy density of petroleum fuels [3]. Recently, the utilization of coffee ground has been attempted as a new resource because of the growth

of coffee consumption worldwide. The coffee consumption for 2019/20 worldwide is forecasted to be 10.2 million tons per year according to the U.S. Department of Agriculture [5]. After the coffee brewing, about 99% of the original amount is wasted as coffee ground. Some of this residue has been utilized as compost or deodorant, but most of them become municipal waste and extra cost is needed to treat by incineration or landfill. The advantages of utilizing coffee ground as an energy source are not only in reducing waste but also in contributing to resolving the global warming problem.

In previous studies on the bio-crude oil from coffee ground [6,7], it was found that the bio-crude oil from coffee ground has a considerably larger calorific value than that from woody biomass. But the viscosity of the bio-crude oil from coffee ground is quite high and it increases with time which could even impede its flow [7]. Combustion characteristics of bio-crude oil have been studied in thermal and power devices including industrial boilers, gas turbines, and diesel engines [8–14]. It was found that the direct application of bio-crude oil to conventional combustors could not be practical mainly due to the clogging problems in the fuel injection system which originates from the high viscosity of bio-crude oil [9].

To overcome the clogging problem in a precise fuel orifice which is generally used in conventional combustors, air-blast nozzles have been tested with a larger diameter for liquid injection [15–17]. To further improve the spray behavior and flame stability, it has been suggested to blend bio-crude oil with ethanol [16–19]. Although a stable combustion of bio-crude oil from woody biomass has been achieved with up to 90% of bio-crude oil by volume [15], the combustion characteristics of bio-crude oil from coffee ground are expected to be quite different from those from sawdust bio-crude oil due to its considerably larger viscosity. In this study, a pilot-scale burner system was developed for the combustion of bio-crude oil from coffee ground. The temperature distributions in the combustion chamber and the gaseous emissions were compared at various experimental conditions including the atomizing air pressure, swirl intensity, and overall equivalence ratio to find out the optimum condition for flame stability and minimum gaseous emissions.

2. Materials and Methods

2.1. Burner System Setup

A bio-crude oil burner system was developed with a capacity of 35 kW as shown in Figure 1. The burner system consisted of the fuel nozzle, the variable swirl generator of combustion air, the fuel tank and preheating line, the air compressor for the fuel atomizing air, and the fan for the combustion air. The burner system adopts a downward injection type where the fuel is supplied from the top of the combustion chamber to the downward direction. In the downward injection burner system, the heat transfer from the flame to the fuel spray can enhance the ignition characteristics, and the combustion efficiency can be improved due to the longer residence time of the fuel in the combustion chamber.

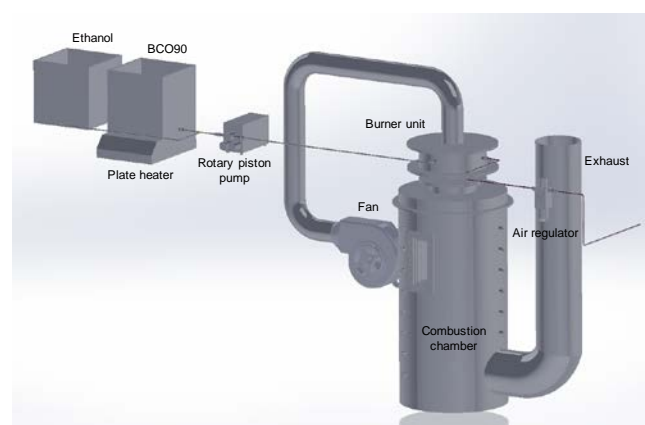


Figure 1. Bio-crude oil burner setup.

Bio-crude oil was produced from the fast pyrolysis of coffee ground in the tilted-slide reactor [7]. The viscosity of bio-crude oil is known to be much higher than that of the petroleum fuel [1,3]. In particular, the bio-crude oil from coffee ground has a significantly high viscosity in comparison with that from woody biomass [7]. The high viscosity of fuel can cause the clogging of the fuel supply line and the fuel nozzle. Furthermore, the quality of fuel spray is degraded due to the increase of the droplet size. It is known that the viscosity can be reduced by mixing alcohol or by increasing temperature [15–20]. The fuel properties will be discussed in detail in the next subsection.

The schematic of the burner unit including the fuel nozzle and the swirl generator is shown in Figure 2a. In this study, an external mix air-blast spray nozzle is made by arranging concentric double tubes with different diameters. The fuel nozzle was placed on the centerline of the burner unit as shown in Figure 2a. The outer diameter (o.d.) and inner diameter (i.d.) of the inner tube for fuel supply are 6.35 mm and 4.57 mm, respectively. The o.d. and i.d. of the outer tube for atomizing air supply are 9.53 mm and 6.83 mm, respectively. The fuel is injected from the inner tube, and the atomizing air flows through the rim shape slit which is formed between the inner and outer tubes. The slit width for the air flow is 0.24 mm. The fuel column disperses into spray droplets by the surrounding air flow with a high velocity [21]. The fuel flow rate from the reservoir to the nozzle was controlled by a rotary piston pump. Atomizing air was supplied from an air compressor and the pressure was controlled by an air regulator.

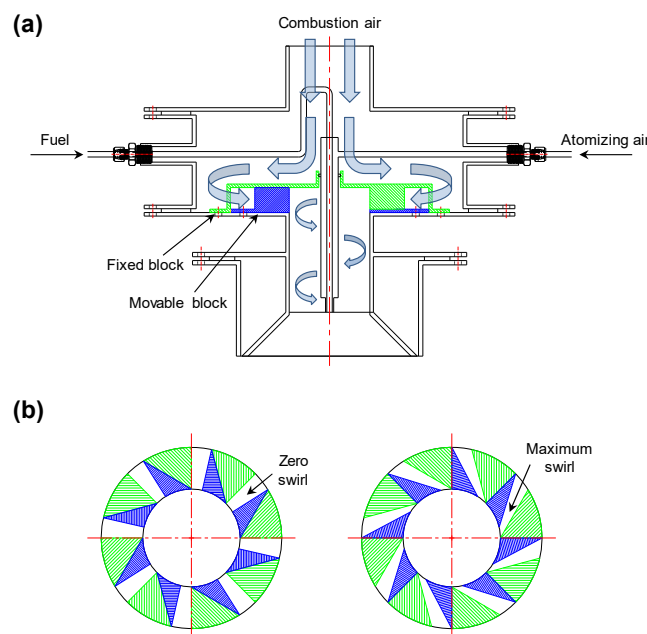


Figure 2. Schematic of burner unit (a) and movable block swirl generator (b).

Swirl flow was generated for the combustion air by adopting a movable block swirl generator [22–25] as shown in Figure 2a,b. It is known that a recirculation zone is formed by the swirling air flow, which supports the flame stability as well as the ignition of fuel spray [26]. The swirl intensity can be varied by the rotation angle of the movable block as shown in Figure 2b. The swirl number S can be evaluated using the parameters such as number of swirl blocks, swirl generator radius, depth and angle of swirl block, maximum opening angle as follows [27]:

$$S \approx \frac{2\pi}{n\xi_m} \cdot \sin \alpha \cdot \frac{\cos \alpha [1 + \tan \alpha \tan(\xi/2)] (\xi/\xi_m)}{\{1 - [1 - \cos \alpha (1 + \tan \alpha \tan(\xi/2)) \xi/\xi_m]\}^2} \cdot \frac{R}{2B} \left[1 - \left(\frac{R_h}{R} \right)^2 \right] \quad (1)$$

where the parameters for calculating the swirl number are listed in Table 1.

The diameter of the burner unit was 10 cm, and a burner quarl was introduced with 45 expansion angle at the combustion air exit. The diameter and the height of the combustion chamber are 40 cm and 90 cm, respectively. The combustion chamber was surrounded by ceramic fiber (5 cm thick) for thermal insulation. A viewport was installed near the fuel nozzle exit to observe the flame behavior. The flame images have been obtained by a digital camera (Nikon D300).

Table 1. Parameters for evaluating the swirl number.

Parameter	Description	Value
n	Number of swirl blocks	8
R	Swirl generator exit radius	46.8 mm
R_h	Swirl generator inner radius	9.5 mm
B	Depth of swirl blocks	25 mm
α	Fixed swirl block angle	60°
ξ	Adjustable swirl block angle	-
ξ_m	Maximum opening angle	12.8°

For the burner startup, the combustion chamber was preheated for approximately 30 min by using pure ethanol to reach a sufficient temperature to ignite the bio-crude oil and ethanol mixture. K-type thermocouples were installed in the combustion chamber as shown in Figure 3. The thermocouples numbered 1–7 are installed at 10 cm from the top, and those numbered by 8–14, 15–21, etc. are located at 10 cm intervals below. The thermocouples in the radial direction have a distance of 10 cm from the center. The number (0) in Figure 3a indicates that a thermocouple is not installed because of the viewport or exhaust as shown in Figure 3b. The temperatures in the combustion chamber were monitored by a data logger (GL820 midi LOGGER) every minute. The accuracy of K-type thermocouple is $\pm 0.75\%$. When the temperature of each test case was stabilized after 15–20 min, the gaseous emissions were measured at a specified location in the exhaust using a gas analyzer (MRU NOVA 2000). Before finishing the experiment, the nozzle and the fuel supply line was flushed by supplying pure ethanol for about 10 min.

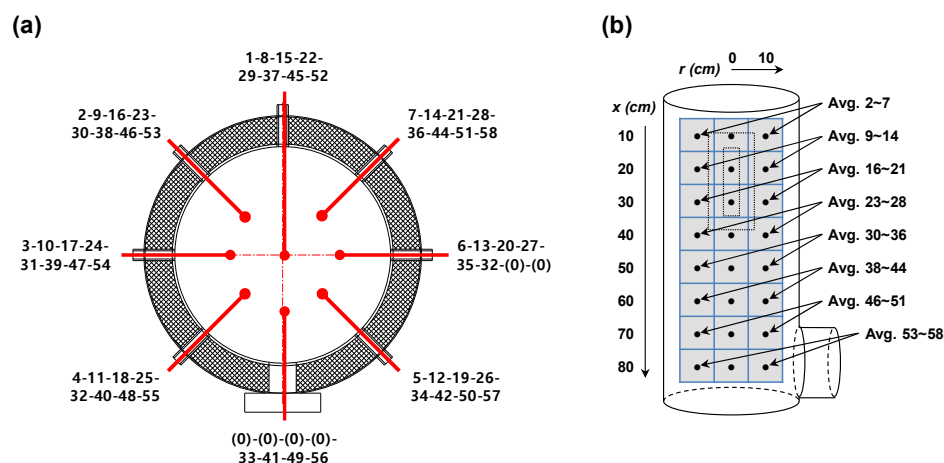


Figure 3. Thermocouple positions in the combustion chamber in top view (a), temperature averaging in 2D axisymmetry (b).

2.2. Fuel Properties

In this study, bio-crude oil from coffee ground was blended with ethanol to improve its spray behavior and flame stability. Although a higher ethanol mixing ratio could guarantee better combustion characteristics, the extra cost of the ethanol should be taken into consideration. Therefore, it is important not only to achieve the flame stability but also to minimize the amount of ethanol. The volumetric mixing ratio of bio-crude oil and ethanol was selected at 90:10 (referred to as BCO90) which is based

on the suggested value for the minimal amount of ethanol in the previous study for sawdust bio-crude oil [15], and the ethanol mixing ratio larger than 10% (e.g., BCO85) has not been taken into account in this study. BCO95 has been also tested although the results have not been shown in detail, and it was found that CO emission was too large (>5000 ppm) arising from higher degree of incomplete combustion which is undesirable in combustion devices. Therefore, the optimum mixing ratio of ethanol could be suggested to be 10% (BCO90).

The thermophysical properties including higher heating values (HHV), viscosities, and densities of bio-crude oil from coffee ground and its mixture with ethanol (BCO90) are listed in Table 2. The elemental compositions are also shown. The higher heating values were measured by a bomb calorimeter (LECO AC-350) following ASTM D2015, and the elemental compositions were measured by an elemental analyzer (Flash EA 1112 series). The properties of sawdust bio-crude oil in the previous study [15] are compared for reference. The BCO90 from coffee ground has larger contents of carbon and hydrogen while it has smaller oxygen content than the sawdust bio-crude oil, which leads to higher HHV than that of sawdust bio-crude oil by about 30%.

The volumetric fuel flow rate corresponding to burner capacity of 35 kW was determined by the heating value and density of the fuel blend (BCO90). The lower heating value (LHV) of BCO90 can be calculated using its higher heating value (HHV) and hydrogen content (H) as follows [15,28]:

$$\text{LHV}_{\text{ar}} [\text{MJ}/\text{kg}] = \text{HHV}_{\text{ar}} [\text{MJ}/\text{kg}] - 2.443 [\text{MJ}/\text{kg}] \times \frac{8.936\text{H}_{\text{ar}}}{100} \quad (2)$$

where the subscript ar indicates as received material. The values of 2.443 and 8.936 correspond to the heat of vaporization of water and the ratio of water produced by combustion to the hydrogen content of the material in weight percent, respectively. Substituting the values of HHV_{ar} and H_{ar} of BCO90 into Equation (2), the LHV_{ar} of the BCO90 was calculated to be 20.03 MJ/kg. The volumetric LHV for adjusting the pump flow rate was determined to be 20.63 MJ/L.

Table 2. Properties of the coffee bio-crude oil (BCO)100, 90 and sawdust BCO [15] (wet basis).

Fuel	HHV (MJ/kg)	Viscosity (cP at 50 °C)	Density (kg/L)	Elemental Composition (wt%)				
				C	H	O ¹	N	S
Coffee BCO	21.14	862.3	1.06	47.12	7.72	41.08	4.08	0
Coffee BCO90	21.80	373.4	1.03	47.51	8.13	40.59	3.77	0
Sawdust BCO [15]	16.75	22.9	1.20	41.07	7.84	50.91	0.19	0

¹ The oxygen content has been calculated as the difference between 100 and the sum of other elements.

It is known that the viscosity of bio-crude oil is quite sensitive to the temperature [3,7,15], and the viscosities of BCO90 at various temperatures were compared in Figure 4. The viscosity was measured by a viscometer (Brookfield, Model DV-II+ Pro). The viscosity of BCO90 was significantly reduced by increasing its temperature and it decreases by a factor of almost two in every 10 degrees over the range of 30–40 °C and 50–70 °C. Therefore, the fuel blend (BCO90) was preheated up to 70 °C prior to the fuel nozzle. The bottom of the fuel reservoir was heated by a plate heater, and the temperature in the fuel reservoir was evened by using an agitator. The fuel supply line was heated by heating tapes with temperature controllers.

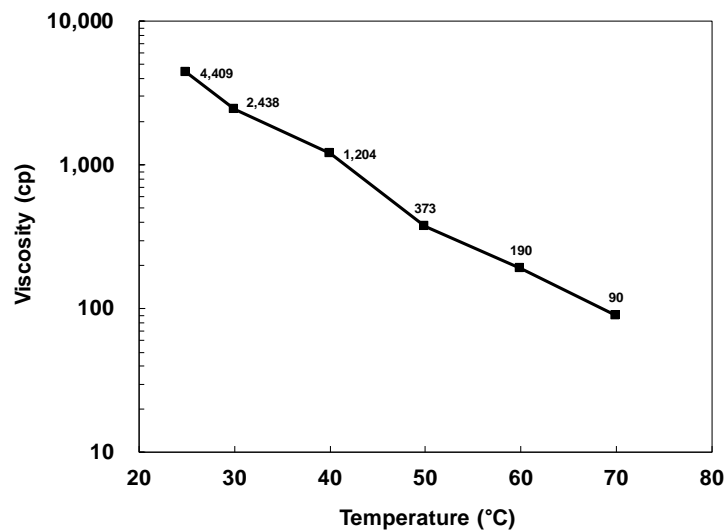


Figure 4. Viscosity of bio-crude oil and ethanol blend (BCO90) at various temperatures.

3. Results and Discussion

The flame images of pure ethanol and BCO90 are shown in Figure 5a,b, respectively. The atomizing air pressure (p), the swirl number (S), and the combustion air flow rate (Q) are same for both cases. The flow rate of $Q = 655$ LPM corresponds to the overall equivalence ratio (ϕ) of 0.8 for BCO90. The ethanol flame shows a light color and a blue chemiluminescence region was observed near the fuel nozzle although not shown directly through the viewport in Figure 5a. On the other hand, the BCO90 flame shows a deep yellow color with a strong radiation as shown in Figure 5b. We note that this radiation contributes to heating which can have advantages in boiler applications. The flame temperature and the gaseous emission are compared for various atomizing air pressures, swirl numbers, and the overall equivalence ratios and the effects of these parameters are investigated.



Figure 5. Direct photos of ethanol flame (a) and BCO90 flame (b) at $p = 100$ kPa, $S = 4.56$, $Q = 655$ LPM.

The temperature distribution inside the combustion chamber is represented in a 2D axisymmetric manner by averaging the values at the same radial distance from the axis. The centerline temperatures (thermocouple numbers 1, 8, 15, 22, 29, 37, 45, 52 in Figure 3a) are kept, while the values on the radial distance of 10 cm (thermocouple numbers 2–7, 9–14, etc.) at the specified axial distance are averaged as shown in Figure 3b.

The O₂, CO, and NO concentrations were measured in the exhaust duct after the flame was stabilized. The average value was used during the continuous measurement for about 3 min. The accuracy of O₂ concentration is ±0.2 vol%, and the accuracy of CO and NO concentrations is ±5% reading. The concentrations CO and NO were normalized as follows:

$$C[\text{ppm}] = C_a[\text{ppm}] \cdot \frac{21 - O_s[\%]}{21 - O_a[\%]} \quad (3)$$

where C , C_a , O_s , and O_a indicate normalized concentration of pollutant, measured concentration of pollutant, standard oxygen concentration, and measured oxygen concentration, respectively. The standard oxygen concentration (O_s) was set at 4% in this study.

3.1. Effect of Atomizing Air Pressure

Figure 6 shows the temperature distribution which is represented in 2D axisymmetry at various atomizing air pressures. The swirl number and the overall equivalence ratio are fixed at $S = 4.56$ and $\phi = 0.8$. The temperature indicated in each cell represents the average value in radial direction or the centerline temperature as shown in Figure 3b. The temperature contour shows a distinct “Λ” shape at the atomizing air pressure of $p = 100$ kPa. The combustion model of spray burning in swirl flows which has been suggested previously [26] can provide a reasonable description of this flame shape. Near the centerline of the atomized jet spray, a low-temperature spray core is formed due to a fuel-rich mixture condition coupled with the quenching effect of the liquid, and the chemical reaction is not significant in this region. The main reaction is placed at the outer periphery of the spray where the air–fuel ratio is near stoichiometry [26]. This flame shape can be observed up to $p = 200$ kPa, but is no longer observed at the largest pressure of $p = 250$ kPa where the centerline temperature becomes larger than the periphery. It can be deduced that at high atomizing air pressure, the characteristic flow timescale is shortened due to the high velocity, which can lead to incomplete chemical reaction. Furthermore, an excessive axial velocity can cause a flame liftoff which can hinder flame stabilization. At $p = 250$ kPa, the temperature near the fuel nozzle sharply decreased to 726 from 939 °C in comparison with the case of $p = 200$ kPa, and it can be observed that the overall temperature level in the combustion chamber declined. Therefore, in this study it can be suggested that the atomizing air pressure should be less than 250 kPa to achieve combustion efficiency and flame stability. Nevertheless, it should be noted that when the air pressure is too low, the fuel droplet size becomes larger which can lead to a poor spray quality. The empirical formula of the Sauter mean diameter (SMD) in air-blast atomizer can be expressed as follows [21]:

$$\text{SMD} = 0.95 \left[\frac{(\sigma_L W_L)^{0.33}}{U_R \rho_L^{0.37} \rho_A^{0.30}} \right] \left[1 + \frac{W_L}{W_A} \right]^{1.70} + 0.13 \mu_L \left[\frac{D_0}{\sigma_L \rho_L} \right]^{0.5} \left[1 + \frac{W_L}{W_A} \right]^{1.70} \quad (4)$$

where σ_L , ρ_L , ρ_A , U_R , W_L , W_A , μ_L , D_0 are surface tension of liquid, density of liquid, density of air, relative velocity of air to liquid, mass flow rate of liquid, mass flow rate of air, dynamic viscosity of liquid, and the liquid orifice diameter, respectively. From this expression, it can be known that the mean droplet size decreases when the relative velocity of air to liquid (U_R) and the mass flow rate of air (W_A) increases which is directly related to the atomizing air pressure. Although not shown, when the atomizing air pressure was reduced to less than 100 kPa it was observed that some of the unburned fuel droplets attached on the viewport inner surface.

The O₂ concentration generally increases with pressure except for the range of 150–200 kPa as shown in Figure 7. The normalized CO concentration decreases with the atomizing air pressure whereas the normalized NO concentration increases. The NO emission is much larger than the case of sawdust bio-crude oil [17] which was slightly larger than 100 ppm. We note that there is a considerable amount of nitrogen in the bio-crude oil from coffee ground (3.77%) as shown in Table 2, which can be a source of Fuel NO. Because there is a trade-off between CO and NO emissions with the atomizing air

pressure, the optimum range of the atomizing air pressure for minimizing the gaseous emissions can be suggested to be $p = 150\text{--}200$ kPa.

$p = 100$ kPa			$p = 150$ kPa			$p = 200$ kPa			$p = 250$ kPa		
940	1028	940	934	886	934	916	939	916	866	726	866
1020	1049	1020	1002	1001	1002	974	977	974	913	914	913
1034	1044	1034	1007	1004	1007	991	983	991	942	972	942
1026	1015	1026	996	981	996	987	972	987	955	969	955
1024	1011	1024	992	978	992	990	979	990	959	964	959
1009	1006	1009	979	973	979	982	984	982	950	957	950
993	983	993	964	954	964	975	970	975	939	939	939
988	982	988	962	957	962	977	975	977	934	934	934

Figure 6. Temperature distributions for various atomizing air pressures at $S = 4.56$ and $\phi = 0.8$.

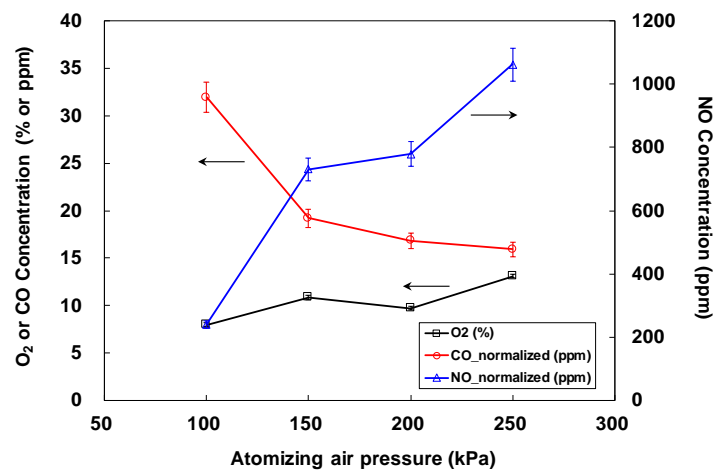


Figure 7. O₂ concentration (%), normalized CO and NO concentrations (ppm) for various atomizing air pressures at $S = 4.56$ and $\phi = 0.8$.

3.2. Effect of Swirl Number

The temperature distributions for various swirl numbers are shown in Figure 8. The atomizing air pressure and the overall equivalence ratio are fixed at $p = 150$ kPa and $\phi = 0.8$. When there is no swirl in the combustion air ($S = 0$), the high temperature region is concentrated far from the nozzle. As the swirl number increases, the high temperature region moves upstream. This transition is clearly observed from $S = 1.25$ to $S = 2.53$. It is interesting to note that the temperature contour resembles “U” shape at $S = 2.53$, and it is transformed into “ Λ ” shape at $S = 4.56$ due to the shift of the high temperature region toward the upstream direction as the swirl number increases.

S = 0			S = 0.46			S = 1.25			S = 2.53			S = 4.56		
881	721	881	858	743	858	863	782	863	877	808	877	934	886	934
916	894	916	900	888	900	906	951	906	927	947	927	1002	1001	1002
944	948	944	934	952	934	940	1009	940	975	969	975	1007	1004	1007
968	972	968	966	980	966	971	996	971	982	964	982	996	981	996
992	989	992	991	994	991	993	1000	993	987	976	987	992	978	992
995	994	995	995	997	995	998	1005	998	983	983	983	979	973	979
991	984	991	991	988	991	994	996	994	975	971	975	964	954	964
997	993	997	997	994	997	1000	1000	1000	977	976	977	962	957	962

Figure 8. Temperature distributions for various swirl numbers at $p = 150$ kPa and $\phi = 0.8$.

When there is enough swirl motion, the recirculation zone is created where the hot combustion products are circulated back toward the fuel nozzle. This effect can greatly enhance the flame stabilization in comparison with no swirl case. Furthermore, the recirculation zone with high temperature can also promote the ignition of the fuel spray.

The O_2 concentration does not vary much with the swirl number as shown in Figure 9. For CO emission, there cannot be observed a consistent tendency in the range from $S = 0.46$ to 4.56 but the CO level increases sharply in the zero swirl case. The large CO concentration indicates that an incomplete combustion is more significant when there is no swirl in the combustion air. The NO concentration is largest at zero swirl and decreases continuously with increasing swirl number. The results of temperature and NO concentration suggests that the maximum swirl intensity is optimum not only for the flame stabilization but also for reducing NO emission in the combustion of bio-crude oil from coffee ground.

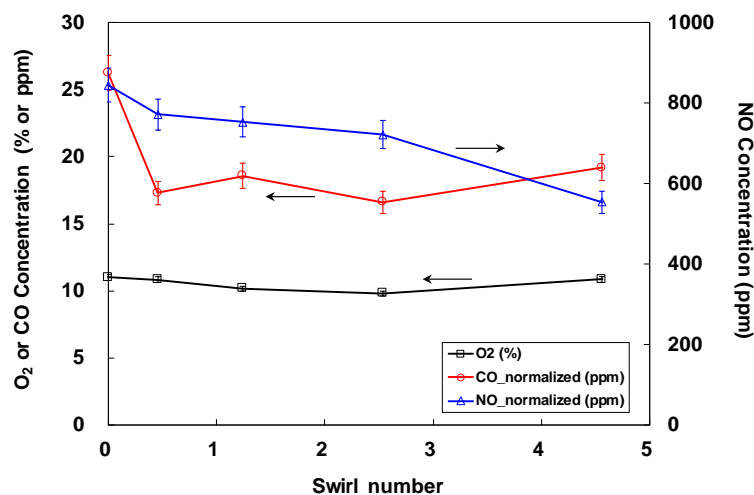


Figure 9. O_2 concentration (%), normalized CO and NO concentrations (ppm) for various swirl numbers at $p = 150$ kPa and $\phi = 0.8$.

3.3. Effect of Overall Equivalence Ratio

Figure 10 shows the temperature distribution for various overall equivalence ratios at $p = 150$ kPa and $S = 4.56$. The average temperature level is lowest at $\phi = 0.5$ although a high temperature region is locally observed near the fuel nozzle ($T = 1012$ °C at $x = 10$ cm, $r = 0$ cm). The lower temperature at smaller ϕ is due to higher dilution of the fuel-air mixture. The temperature level increases when the overall equivalence ratio becomes closer to stoichiometry. The contour of high temperature is more concentrated in the downstream region at the condition of $\phi = 0.5$, which indicates that the primary reaction zone is pushed away from the fuel nozzle because of the large air velocity. The high

temperature region migrates upstream as increasing overall equivalence ratio. It is interesting to note that the local maximum near the fuel nozzle ($x = 10$ cm, $r = 0$ cm) at $\phi = 0.5$ disappears at larger ϕ , and the temperature at this point becomes smaller with increasing ϕ . It might be thought that there can be formed a small but strong recirculation zone near the fuel nozzle a when the swirling air flow rate is excessively high, which can form a local strong reaction zone near the fuel jet core. A further investigation would be useful for a future study.

$\phi = 0.5$			$\phi = 0.6$			$\phi = 0.7$			$\phi = 0.8$		
759	1012	759	898	953	898	964	952	964	934	886	934
924	953	924	976	964	976	981	970	981	1002	1001	1002
948	937	948	984	968	984	984	980	984	1007	1004	1007
939	917	939	977	957	977	984	974	984	996	981	996
950	932	950	979	964	979	992	983	992	992	978	992
951	941	951	971	967	971	985	987	985	979	973	979
951	936	951	962	953	962	979	971	979	964	954	964
961	951	961	964	958	964	982	976	982	962	957	962

Figure 10. Temperature distributions for various overall equivalence ratios at $p = 150$ kPa and $S = 4.56$.

The O_2 concentration does not vary much with the overall equivalence ratio as shown in Figure 11. The normalized CO concentration is similar at $\phi = 0.5$ and 0.6 , and is reduced sharply at $\phi = 0.7$ while is increased at $\phi = 0.8$. The normalized NO concentration is also similar at $\phi = 0.5$ and 0.6 but it decreases from $\phi = 0.6$ to 0.8 . On the aspect of minimizing the pollutant emission, the optimum condition for the overall equivalence ratio is suggested to be in the range of $\phi = 0.7-0.8$ in this study.

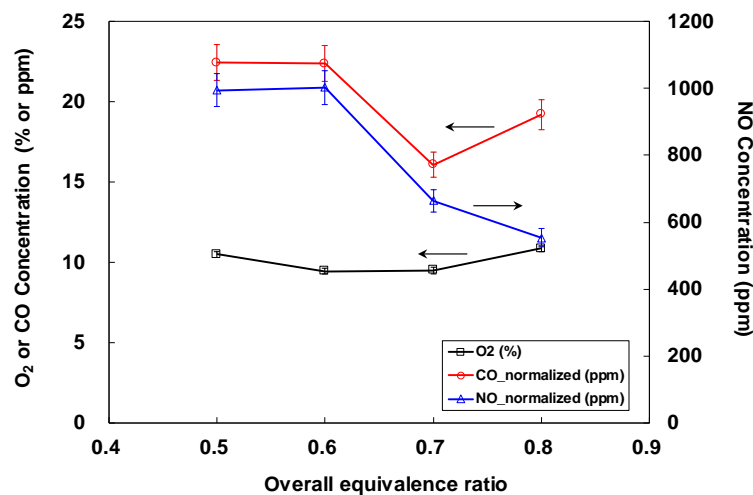


Figure 11. O_2 concentration (%), normalized CO and NO concentrations (ppm) for various overall equivalence ratios at $p = 150$ kPa and $S = 4.56$.

Through the results of temperature distributions and gaseous emissions at various atomizing air pressures, swirl numbers, and overall equivalence ratios, the best operating conditions for the bio-crude oil burner can be suggested as follows. When the atomizing air pressure is too high, the flame can be unstable due to the incomplete chemical reaction and flame liftoff. But too low pressure can lead to an excessively larger droplet size and a poor spray quality. The best condition of atomizing air pressure ranges from 150 kPa to 200 kPa. In case of swirl number, a higher swirl intensity can enhance the flame stability by promoting the recirculation zone of the hot combustion products. NO emission was also decreased with a higher swirl number. The effect of overall equivalence ratio can

be summarized that when the equivalence ratio is too low, the flame temperature in the combustion chamber is reduced due to higher dilution which can degrade the burner performance. An excessively large flow rate of the combustion air can also lead to an unstable combustion and larger NO emission. The overall equivalence ratio from 0.7 to 0.8 is suggested for the best operating condition in this study.

4. Conclusions

A spray burner system with capacity of 35 kW was developed for the combustion of bio-crude from coffee ground. The bio-crude oil was blended with ethanol at the volumetric ratio of bio-crude oil to ethanol of 9:1, and the fuel was supplied through an air-blast spray nozzle which has a relatively large nozzle diameter which is suitable for large viscosity fuels. A burner system with downward injection type was adopted to enhance the spray and ignition characteristics, and swirl flow was introduced to the combustion air to promote the combustion stability. The temperature distributions and the gaseous emissions are investigated at various atomizing air pressure, swirl number, and overall equivalence ratios. The results for the effect of atomizing air pressure suggests that the air pressure should be in the range of 150 kPa to 200 kPa to achieve a flame stability and minimum gaseous emissions. The higher swirl motion in the combustion air is found to be better not only for the flame stabilization and smaller gaseous emissions. The optimum overall equivalence ratio could be suggested between 0.7 and 0.8 to minimize the gaseous emissions in this study.

Author Contributions: Conceptualization, Y.S.C.; Data curation, S.Y.H. and Q.V.N.; Investigation, S.K.C. and Y.W.J.; Methodology, S.K.C. and Y.W.J.; Project administration, Y.S.C.; Resources, S.Y.H.; Supervision, Y.S.C.; Visualization, Q.V.N.; Writing—original draft, S.K.C. All authors have read and agreed to the published version of the manuscript.

Funding: This work was supported by the “Development of Rooftop WISE Farm Technologies Utilizing Building Energy” project (NK219G) of the Korea Institute of Machinery and Materials under the auspices of the Korea government (MSIT), Republic of Korea. This work was also supported by the National Research Council of Science & Technology (NST) grant by the Korea government (MSIT) No. CAP-16-05-KIMM. The authors gratefully acknowledge this support.

Conflicts of Interest: The authors declare no conflict of interest.

References

1. Bridgwater, A.V. Review of fast pyrolysis of biomass and product upgrading. *Biomass Bioenergy* **2012**, *38*, 68–94. [CrossRef]
2. Bridgwater, A.V.; Meier, D.; Radlein, D. An overview of fast pyrolysis of biomass. *Org. Geochem.* **1999**, *30*, 1479–1493. [CrossRef]
3. Lu, Q.; Li, W.Z.; Zhu, X.F. Overview of fuel properties of biomass fast pyrolysis oils. *Energy Convers. Manag.* **2009**, *50*, 1376–1383. [CrossRef]
4. Mohan, D.; Pittman, C.U.; Steele, P.H. Pyrolysis of wood/biomass for bio-oil: A critical review. *Energy Fuels* **2006**, *20*, 848–889. [CrossRef]
5. USDA Foreign Agricultural Service. *Coffee: World Markets and Trade*; 2019; pp. 1–9. Available online: <https://www.fas.usda.gov/data/coffee-world-markets-and-trade> (accessed on 29 April 2020).
6. Bok, J.P.; Choi, H.S.; Choi, Y.S.; Park, H.C.; Kim, S.J. Fast pyrolysis of coffee grounds: Characteristics of product yields and biocrude oil quality. *Energy* **2012**, *47*, 17–24. [CrossRef]
7. Choi, Y.S.; Choi, S.K.; Kim, S.J.; Jeong, Y.W.; Soysa, R.; Rahman, T. Fast pyrolysis of coffee ground in a tilted-slide reactor and characteristics of biocrude oil. *Environ. Prog. Sustain. Energy* **2017**, *36*. [CrossRef]
8. Chiamonti, D.; Oasmaa, A.; Solantausta, Y. Power generation using fast pyrolysis liquids from biomass. *Renew. Sustain. Energy Rev.* **2007**, *11*, 1056–1086. [CrossRef]
9. Lee, S.; Kim, T.; Kang, K. Performance and emission characteristics of a diesel engine operated with wood pyrolysis oil. *Proc. Inst. Mech. Eng. Part D J. Automob. Eng.* **2014**, *228*, 180–189. [CrossRef]
10. López Juste, G.; Salvá Monfort, J.J. Preliminary test on combustion of wood derived fast pyrolysis oils in a gas turbine combustor. *Biomass Bioenergy* **2000**, *19*, 119–128. [CrossRef]

11. Oasmaa, A.; Kyto, M.; Sipila, K. Pyrolysis oil combustion tests in an industrial boiler. In *Progress in Thermochemical Biomass Conversion*; Bridgwater, A.V., Ed.; Blackwell Science: Oxford, UK, 2001; pp. 1468–1481.
12. Shihadeh, A.; Hochgreb, S. Diesel engine combustion of biomass pyrolysis oils. *Energy Fuels* **2000**, *14*, 260–274. [[CrossRef](#)]
13. Solantausta, Y.; Nylund, N.-O.; Gust, S. Use of pyrolysis oil in a test diesel engine to study the feasibility of a diesel power plant concept. *Biomass Bioenergy* **1994**, *7*, 297–306. [[CrossRef](#)]
14. Strenziok, R.; Hansen, U.; Kunstner, H. Combustion of bio-oil in a gas turbine. In *Progress in Thermochemical Biomass Conversion*; Bridgwater, A.V., Ed.; Blackwell Science: Oxford, UK, 2001; pp. 1452–1458.
15. Choi, S.K.; Choi, Y.S.; Kim, S.J.; Jeong, Y.W. Characteristics of flame stability and gaseous emission of biocrude-oil/ethanol blends in a pilot-scale spray burner. *Renew. Energy* **2016**, *91*, 516–523. [[CrossRef](#)]
16. Tzanetakis, T.; Farra, N.; Moloodi, S.; Lamont, W.; McGrath, A.; Thomson, M.J. Spray combustion characteristics and gaseous emissions of a wood derived fast pyrolysis liquid-ethanol blend in a pilot stabilized swirl burner. *Energy Fuels* **2010**, *24*, 5331–5348. [[CrossRef](#)]
17. Zheng, J.L.; Kong, Y.P. Spray combustion properties of fast pyrolysis bio-oil produced from rice husk. *Energy Convers. Manag.* **2010**, *51*, 182–188. [[CrossRef](#)]
18. Martin, J.A.; Boateng, A.A. Combustion performance of pyrolysis oil/ethanol blends in a residential-scale oil-fired boiler. *Fuel* **2014**, *133*, 34–44. [[CrossRef](#)]
19. Nguyen, D.; Honnery, D. Combustion of bio-oil ethanol blends at elevated pressure. *Fuel* **2008**, *87*, 232–243. [[CrossRef](#)]
20. Stamatov, V.; Honnery, D.; Soria, J. Combustion properties of slow pyrolysis bio-oil produced from indigenous Australian species. *Renew. Energy* **2006**, *31*, 2108–2121. [[CrossRef](#)]
21. Lefebvre, A.H. Airblast atomization. *Prog. Energy Combust. Sci.* **1980**, *6*, 233–261. [[CrossRef](#)]
22. Ballester, J.; Barroso, J.; Cerecedo, L.M.; Ichaso, R. Comparative study of semi-industrial-scale flames of pulverized coals and biomass. *Combust. Flame* **2005**, *141*, 204–215. [[CrossRef](#)]
23. Palm, R.; Grundmann, S.; Weismüller, M.; Šarić, S.; Jakirlić, S.; Tropea, C. Experimental characterization and modelling of inflow conditions for a gas turbine swirl combustor. *Int. J. Heat Fluid Flow* **2006**, *27*, 924–936. [[CrossRef](#)]
24. Ćosić, B.; Bobusch, B.C.; Moeck, J.P.; Paschereit, C.O. Open-loop control of combustion instabilities and the role of the flame response to two-frequency forcing. *J. Eng. Gas Turbines Power* **2012**, *134*, 1–8. [[CrossRef](#)]
25. Jones, W.P.; Marquis, A.J.; Prasad, V.N. LES of a turbulent premixed swirl burner using the Eulerian stochastic field method. *Combust. Flame* **2012**, *159*, 3079–3095. [[CrossRef](#)]
26. Gupta, A.K.; Lilley, D.G.; Syred, N. *Swirl Flows*; Energy and engineering science series; Abacus Press: Tunbridge Wells, Kent, UK, 1984; ISBN 9780856261756.
27. Fudihara, T.J.; Goldstein, L.; Mori, M. The three-dimensional numerical aerodynamics of a movable block burner. *Braz. J. Chem. Eng.* **2003**, *20*, 391–401. [[CrossRef](#)]
28. Hodgson, E.M.; Fahmi, R.; Yates, N.; Barraclough, T.; Shield, I.; Allison, G.; Bridgwater, A.V.; Donnison, I.S. Miscanthus as a feedstock for fast-pyrolysis: Does agronomic treatment affect quality? *Bioresour. Technol.* **2010**, *101*, 6185–6191. [[CrossRef](#)]

